

Imaging resonances in low-energy NO-He inelastic collisions

Sjoerd N. Vogels*, Jolijn Onvlee*, Simon Chefdeville, Ad van der Avoird, Gerrit C. Groenenboom**, Sebastiaan Y.T. van de Meerakker**

Radboud University, Institute for Molecules and Materials
Heijendaalseweg 135, 6525 AJ Nijmegen, the Netherlands

*Who contributed equally to this work;

**To whom correspondence should be addressed;

E-mail: basvdm@science.ru.nl, gerritg@theochem.ru.nl

In molecular collisions, resonances occur at specific energies where the colliding particles temporarily form quasi-bound complexes, resulting in rapid variations in the energy dependence of scattering cross sections. Experimentally, it has proven challenging to observe such scattering resonances, especially in differential cross sections. We report the observation of resonance fingerprints in the state-to-state differential cross sections for inelastic NO-He collisions in the 13 to 19 cm⁻¹ energy range with 0.3 cm⁻¹ resolution. The observed structures were in excellent agreement with quantum scattering calculations. They were analyzed by separating the resonance contributions to the differential cross sections from the background through a partitioning of the multichannel scattering matrix. This revealed the partial wave composition of the resonances, and their evolution during the collision.

Acquiring a detailed understanding of interactions between individual molecules is of fundamental importance to physics and chemistry, and has a long and rich tradition. Historically, two distinct types of experiments have been conducted to unravel the precise nature of inter- and intramolecular forces. On the one hand, spectroscopic studies yield information on the binding forces that hold the molecule together, as well as on the noncovalent interactions between the molecules. They mainly probe the shape of the interaction potential in the region of the well. Collision experiments, on the other hand, are typically more sensitive to the short range repulsive part of the potential.

Certainly, the interactions between microscopic objects such as atoms and molecules require a full quantum mechanical description. In contrast with molecular spectra, where the discrete lines and bands directly reveal the quantized energy levels of the molecule, the quantum nature of molecular collisions is more subtle. In addition to the internal states of the molecule, the angular momentum associated with the relative motion of the particles is also quantized. This relative motion is described by a set of partial waves with integer quantum number ℓ (l).

Unraveling the contribution of each individual partial wave to a collision cross section would provide the ultimate information that can be retrieved from any collision event. Experimentally, however, it is impossible to select a single partial wave from the pre-collision conditions, and to study how the interaction transforms it into post-collision properties. The number of contributing partial waves depends on the de Broglie wavelengths of the particles; observable quantities such as scattering cross sections therefore necessarily represent the quantum mechanical superposition of many partial waves (2). Classically, this can be compared to the unavoidable averaging over all possible impact parameters of the two colliding particles (l).

At low temperatures, special conditions exist where a single partial wave can dominate the scattering process, mitigating this fundamental obstacle. When the collision energy is resonant with a quasi-bound state supported by the interaction potential, the incident particles can

temporarily form a long-lived complex. At these energies, a resonant partial wave ℓ_{res} may dominate over all other partial waves, and there will be a strong enhancement of the scattering cross section. For atom-molecule collisions, these so-called scattering resonances may be regarded — in a simplified picture — either as the orbiting of the atom around the molecule (a shape or orbiting resonance), or as the transient excitation of the molecule to a state of higher energy (a Feshbach resonance). After some time, however, the complex falls apart and decays back into a separate atom and molecule (3).

Scattering resonances are the most global and sensitive probes of molecular interaction potentials. They depend on both the long range attractive and the short range repulsive part of the potential, as well as on the van der Waals well; they are not only sensitive to the shape of the well — as are the spectra of molecular complexes — but also to the depth of the well relative to the dissociation limit. Measurements of the resonance position and width in the integral cross section (ICS) probe the energy and lifetime of the quasi-bound state from which the resonance originates. Such observations may thus be regarded as a type of collision spectroscopy. Still, they do not yield information on the partial wave composition of the resonance. More information on the collision dynamics is inferred from the differential cross section (DCS) at the resonance energy. The structured DCS represents the partial wave fingerprint of the collision process, and offers at the resonance the opportunity to experimentally probe the relation between incoming, resonant, and outgoing partial waves. This gives detailed insights into the most fundamental question in molecular collision dynamics: how does the interaction potential transform the reagents into the collision products?

Whereas scattering resonances are well-known in electron, neutron and ultracold atom scattering, the observation of scattering resonances in molecular systems has been a quest for decades. Experimentally, it has proven extremely challenging to reach the required low collision energies and high energy resolution to observe and characterize partial wave resonances.

In crossed beam experiments, signatures of scattering resonances have been observed in reactive systems with a low excitation barrier, such as the benchmark $F + H_2$ and $F + HD$ reactions, using the powerful Rydberg tagging technique to record the angular distribution of the H or D products (4–10). In these systems, the resonance is associated with the formation of transiently stable transition-state structures. High-resolution anion photodetachment spectroscopy in combination with accurate calculations has recently allowed the observation and characterization of previously unresolved reactive scattering resonances in this system (11). Using a merged beam approach, resonances have recently also been observed in ICSs for Penning ionization processes at collision temperatures in the mK regime (12, 13). Even more recently, resonances were observed in inelastic scattering processes at energies near the thermodynamic threshold for rotational excitation of the molecule. Using cryogenically cooled molecular species such as CO and O_2 , partial wave resonances were observed in the state-to-state ICSs for inelastic collisions with He and H_2 target beams at energies down to 4 K (14–16).

The measurement of DCSs at scattering resonances remains a largely unexplored frontier, in particular for species other than H and D atoms. At low collision energies, the recoil velocities of the scattered molecules are extremely small, and it has proven a daunting task to obtain the angular resolution required to resolve any deflection structure. Here, we report the measurement of DCSs at partial wave resonances for inelastic collisions between fully state-selected NO radicals [$X^2\Pi_{1/2}, v = 0, j = 1/2, f$ (17), referred to hereafter as (1/2*f*)] and He atoms in a crossed beam experiment. We combined Stark deceleration and velocity map imaging to probe scattering resonances in the state-to-state and parity-resolved DCSs at energies between 13 and 19 cm^{-1} , with a spectroscopic energy resolution of 0.3 cm^{-1} . The high resolution afforded by the Stark decelerator allowed us to observe structure in the very small velocity mapped scattering images, directly reflecting the DCSs. Distinct variations in the DCSs were observed as the collision energy was tuned over the resonances. At off-resonance energies, the DCSs were

dominated by quantum diffraction oscillations, whereas additional strong forward and backward scattering was found at the resonance energies. We developed a theoretical approach similar to Feshbach-Fano partitioning (18, 19) to disentangle the resonance and background contributions to the DCSs, and we directly revealed the incoming and outgoing waves that characterize the resonances and the background.

Collisions between NO and rare gas atoms represent a seminal class of systems in rotational energy transfer, since scattering of open-shell radical species such as NO and OH plays an important role in gas-phase chemical kinetics, combustion, and astrochemistry. Collisions involving these radicals are governed by multiple potential energy surfaces (PESs), parity selection and propensity rules that are foreign to molecules such as CO and O₂ (20). We found excellent agreement with the DCSs predicted by *ab initio* quantum mechanical close-coupling (QM CC) scattering calculations based on accurate NO-He PESs.

We used a crossed molecular beam apparatus with a 45° crossing angle (21). A packet of velocity-controlled NO (1/2*f*) radicals, with a velocity spread of 2.1 m/s (22) and an angular spread of 1.5 mrad, was produced using a 2.6-m long Stark decelerator. The beam of He atoms with a mean velocity between 400 m/s and 480 m/s, a velocity spread of 4.3 m/s and an angular spread of 4.8 mrad was produced by cooling an Even-Lavie valve to cryogenic temperatures. By tuning the NO velocity between 350 m/s and 460 m/s with the Stark decelerator, the collision energy was varied between 13 cm⁻¹ and 19 cm⁻¹ with an energy resolution of 0.3 cm⁻¹. The scattered NO radicals were state-selectively detected using a two-color laser ionization scheme and velocity mapped on a two-dimensional detector.

We studied inelastic collisions that excite the NO (1/2*f*) radicals into either the (3/2*e*) or the (5/2*f*) state. The (5/2*f*) channel opens within the experimentally accessible energy range at 13.4 cm⁻¹, and we measured the threshold behavior in the ICS for this channel to calibrate both the collision energy and energy resolution (shown in Fig. 1A). We observed a plateau just above

threshold and a clear peak around 18 cm^{-1} , which were well reproduced by the theoretical ICS convoluted with the experimental resolution of 0.3 cm^{-1} (21). These features were attributed to a narrow (labeled II) and a broader resonance (labeled III) in the theoretical ICS. The theoretical ICS for the $(3/2e)$ state (shown in Fig. 1B for comparison) showed a clear resonance (labeled I) at a slightly lower energy than resonance II.

For both inelastic channels, scattering images were measured at selected energies (Fig. 2). Depending on the energy and the final state probed, the diameter of the low collision energy images ranged from only a few m/s to about 60 m/s. Note that the diameter of the $(5/2f)$ image approached zero as the energy approached the thermodynamic threshold of the channel, effectively imaging the center of mass velocity of the NO-He pair. Despite their small sizes, distinct structure in the images could clearly be discerned. At higher energies, as illustrated by the additional images probed at 45.0 cm^{-1} , the DCSs of both channels feature a rich diffraction pattern that extends from forward to backward scattering. Each diffraction peak in the DCS transformed into a stripe in the image due to the detection method employed in the experiment. At low collision energies the number of diffraction peaks was reduced, and an additional pattern arose in the vicinity of the resonances. As the energy was varied in small energy steps over the resonances, a strong variation in the angular distribution featuring pronounced forward and backward scattering was observed.

To compare our findings with theoretical predictions, we simulated for each energy the image expected from the kinematics of the experiment and the DCS predicted by high-level QM CC calculations (21). Both the experimental and simulated images were then analyzed to yield the angular scattering distribution, reflecting the DCS convoluted with the experimental energy and angular resolution (21). In general, excellent agreement was found between the experimental and simulated scattering distributions, although at some energies the relative intensities of the observed features differed from the simulated intensities (23).

To interpret our results, we first analyzed the partial wave composition of the scattering cross sections, as well as the scattering wavefunctions (21). We found that for the energies probed, the entrance channel is governed by partial waves up to $\ell_{\text{in}} = 8$. At the resonance energies, however, a single resonant partial wave ℓ_{res} becomes involved in a quasi-bound state, which causes the ICS to rise significantly above the background. We found that resonances I and II are associated with a quasi-bound state of the He-NO($5/2f$) complex at 14.7 cm^{-1} dominated by $\ell_{\text{res}} = 5$, whereas resonance III originates from a He-NO($5/2f$) quasi-bound state at 17.9 cm^{-1} governed by $\ell_{\text{res}} = 6$ (21).

For an inelastic process, the partial wave quantum number ℓ is not conserved throughout the collision. The anisotropic interaction potential couples rotational states of the NO molecule with different quantum numbers j and waves with different values of ℓ , and determines how the incoming waves ℓ_{in} are transformed into the outgoing waves ℓ_{out} during the collision. At the resonance energies, the quasi-bound He-NO($5/2f$) complexes with the well-defined values of $\ell_{\text{res}} = 5$ (resonances I and II) or 6 (resonance III) decomposed to form an NO radical in either the ($3/2e$) state (resonance I) or the ($5/2f$) state (resonances II and III). When the resonant ($5/2f$) state decays into the lower ($3/2e$) state, as for resonance I, not only j but also ℓ changes and ℓ_{out} ranges from 3 to 7 (21). When the final NO state is the same as the resonant state, as for resonances II and III, the dominant value of $\ell_{\text{out}} = 5$ or 6 is the same as ℓ_{res} . At energies just above the threshold of the ($5/2f$) inelastic channel, where almost all kinetic energy has been transferred into rotational energy of the NO molecule, the ($5/2f$) state can only decay with $\ell_{\text{out}} = 0$ (s -wave), $\ell_{\text{out}} = 1$ (p -wave) and $\ell_{\text{out}} = 2$ (d -wave). The observed DCS at 13.8 cm^{-1} was dominated by p -wave scattering with small contributions from s - and d -waves (21).

At the resonance energies, the DCSs contain unique information on the partial wave dynamics of the collision process, i.e., the relation between ℓ_{in} , ℓ_{res} , and ℓ_{out} . If the scattering were purely determined by a resonance without any background, the scattering matrix S

would be given by the Breit-Wigner formula, originally developed for neutron scattering in 1936 and nowadays frequently used to describe scattering processes in high energy particle physics (24, 25). However, in most cases and also in our experiments, the observed ICSs and DCSs result from an interference between resonance and background contributions. We disentangled these contributions for each of the resonances I, II, and III by applying a theoretical analysis similar to Feshbach-Fano partitioning (18, 19). We wrote the energy-dependent multi-channel scattering matrix as (26)

$$\mathbf{S}(E) = \mathbf{S}^{\text{bg}}(E) \mathbf{U}^{\text{res}}(E) \quad (1)$$

where the background contribution $\mathbf{S}^{\text{bg}}(E)$ is a slowly varying function of the collision energy E and the resonance contribution is given by the Breit-Wigner formula

$$\mathbf{U}^{\text{res}}(E) = \mathbf{I} - \frac{2i\mathbf{A}}{E - E_{\text{res}} + i\Gamma} \quad (2)$$

\mathbf{I} is the unit matrix, E_{res} is the energy of the resonance, Γ its width (or inverse lifetime), and the complex-valued matrix elements $A_{\alpha\beta} = a_{\alpha}a_{\beta}^*$ contain the partial widths a_{α} obeying the relation $\sum_{\alpha} |a_{\alpha}|^2 = \Gamma$. The idea associated with the Breit-Wigner formula is that in the complex energy plane, where the bound states correspond to poles of the S -matrix on the negative real energy axis, resonances are represented by poles below the positive real axis at positions $E_{\text{res}} - i\Gamma$. By analyzing the energy dependence of the S -matrix elements in the range of each resonance with an algorithm described in the Supplementary Material (21), we could determine the parameters E_{res} , Γ , and a_{α} . Then, we separated the resonance contributions to the scattering matrix $\mathbf{S}(E)$ from the background and applied the usual expressions (27) to compute the ICS and DCS from the S -matrix, with or without resonance contributions. Figure 3 shows the results for the final ($5/2f$) state of NO, where the effects are most pronounced. The upper panel in this figure demonstrates that the peaks in the ICS corresponding to both resonances II and III vanish when we only included the background contribution. The lower part of this figure illustrates

the effect of the resonances on the DCS at energies close to these resonances. The background contributions (dashed lines) show the usual pattern of diffraction oscillations, which are most pronounced for small scattering angles and decrease in amplitude for larger angles. The effect of the resonance contributions is substantial; they lead to additional strong scattering near the forward and backward directions. Figure 3 also shows a comparison of measured and simulated images at 14.8, 17.1, and 18.2 cm^{-1} . The simulated images were based on DCSs calculated in this energy range, with or without resonance contributions, by taking into account the experimental energy resolution of 0.3 cm^{-1} . Clearly, the experimental images show much better agreement with the simulations when the full DCS is taken into account.

Our theoretical analysis demonstrated that the resonances strongly affect the nature of the DCSs, and allowed us to disentangle normal diffraction oscillations from the resonance fingerprints in the DCSs. The DCSs measured for collision energies in the range of the resonances agreed very well with the DCSs obtained from the *ab initio* calculations, but only when the contributions from the resonances were fully included. This directly confirmed that our experiment indeed images the resonance fingerprints in the DCS.

Our joint experimental and theoretical study showed that scattering resonances in state-to-state cross sections can now be probed with spectroscopic resolution, even for benchmark and chemically relevant systems that involve open-shell species such as NO. DCSs measured at the resonance energies, combined with a theoretical analysis, provided detailed information on the multichannel scattering process and explicitly revealed the effects of the resonances. The theoretical method developed to separate the resonant contributions to the ICSs and DCSs from the background will also be applicable to other systems where scattering resonances occur.

References and Notes

1. The partial wave quantum number ℓ is the quantum mechanical analogue of the classical angular momentum $L = \mu v b$, where μ is the reduced mass, v is the relative velocity of the colliding particles, and b is the impact parameter defined as the distance of closest approach in the absence of any interaction.
2. Single partial wave collisions are only found at temperatures approaching zero kelvin, where the scattering is governed by the wave with the lowest possible value for l . Collisions between ultracold atoms and molecules near quantum degeneracy, for instance, are exclusively governed by partial waves with $l = 0$ (s-wave) or $l = 1$ (p-wave).
3. D. W. Chandler, *J. Chem. Phys.* **132**, 110901 (2010).
4. R. T. Skodje, *et al.*, *Phys. Rev. Lett.* **85**, 1206 (2000).
5. W. Shiu, J. J. Lin, K. Liu, *Phys. Rev. Lett.* **92**, 103201 (2004).
6. M. Qiu, *et al.*, *Science* **311**, 1440 (2006).
7. Z. Ren, *et al.*, *Proc. Natl. Acad. Sci. U.S.A.* **105**, 12662 (2008).
8. W. Dong, *et al.*, *Science* **327**, 1501 (2010).
9. T. Wang, *et al.*, *Science* **342**, 1499 (2013).
10. T. Yang, *et al.*, *Science* **347**, 60 (2015).
11. J. B. Kim, *et al.*, *Science* **349**, 510 (2015).
12. A. B. Henson, S. Gersten, Y. Shagam, J. Narevicius, E. Narevicius, *Science* **338**, 234 (2012).

13. E. Lavert-Ofir, *et al.*, *Nat. Chem.* **6**, 332 (2014).
14. S. Chefdeville, *et al.*, *Phys. Rev. Lett.* **109**, 023201 (2012).
15. S. Chefdeville, *et al.*, *Science* **341**, 1094 (2013).
16. A. Bergeat, J. Onvlee, C. Naulin, A. van der Avoird, M. Costes, *Nat. Chem.* **7**, 349 (2015).
17. The labels $X^2\Pi_{1/2}$, v , and j indicate the electronic state, the vibrational state and rotational state of the NO radical, respectively. Each rotational state of NO possesses two near-degenerate Λ -doublet components, with symmetry labels e (lower component) and f (upper component), that refer to the total parity of the electronic wavefunction, exclusive of rotation.
18. U. Fano, *Phys. Rev.* **124**, 1866 (1961).
19. V. Brems, T. Beyer, B. M. Nestmann, H.-D. Meyer, L. S. Cederbaum, *J. Chem. Phys.* **117**, 10635 (2002).
20. M. Kirste, *et al.*, *Science* **338**, 1060 (2012).
21. Materials and methods are available as supplementary material on *Science Online*.
22. All spreads in this manuscript refer to widths (1σ) of a fitted Gaussian distribution.
23. The calibration of the mean experimental collision energy has an uncertainty of $\pm 0.15 \text{ cm}^{-1}$. Small differences between experimental and simulated images are found in particular at energies where the DCS varies rapidly as a function of collision energy. In addition, the experiment seemed to systematically underestimate the scattering intensity at forward scattering.
24. W. Erlewein, M. von Seggern, J. P. Toennies, *Z. für Physik* **211**, 35 (1968).

25. S. H. Sheen, J. G. Skofronick, C. R. Mueller, *Int. J. Quantum Chem.* **9**, 817 (1975).
26. J. R. Taylor, *Scattering theory: the quantum theory of nonrelativistic collisions (Chapter 20)* (Wiley, New York, 1972).
27. W. A. Lester, Jr., *The N Coupled-Channel Problem* (Plenum Press, New York, 1976), pp. 1–32.
28. J. Onvlee, S. N. Vogels, A. von Zastrow, D. H. Parker, S. Y. T. van de Meerakker, *Phys. Chem. Chem. Phys.* **16**, 15768 (2014).
29. B. Yan, *et al.*, *Rev. Sci. Instrum.* **84**, (2013).
30. U. Even, *Advances in Chemistry* **2014**, 636042 (2014).
31. D. Townsend, M. P. Minitti, A. G. Suits, *Rev. Sci. Instrum.* **74**, 2530 (2003).
32. C. Naulin, N. Daugey, K. M. Hickson, M. Costes, *J. Phys. Chem. A* **113**, 14447 (2009).
33. A. von Zastrow, *et al.*, *Nat. Chem.* **6**, 216 (2014).
34. L. Scharfenberg, *et al.*, *Eur. Phys. J. D* **65**, 189 (2011).
35. J. Kłos, G. Chałasiński, M. T. Berry, R. Bukowski, S. M. Cybulski, *J. Chem. Phys.* **112**, 2195 (2000).
36. A. Gijsbertsen, H. Linnartz, S. Stolte, *J. Chem. Phys.* **125**, 133112 (2006).

Acknowledgement This work is part of the research programme of the Foundation for Fundamental Research on Matter (FOM), which is supported financially by the Netherlands Organization for Scientific Research (NWO). S.Y.T.v.d.M. acknowledges further support from NWO via a VIDI and a TOP grant, and from the European Research Council via a Starting

Grant. We thank André van Roij, Chris Berkhout, Niek Janssen, and Peter Claus for expert technical support. We thank Jacek Kłos for providing us with his NO-He PESs. The authors declare no competing financial interests. Supplementary Material accompanies this paper.

Supplementary Materials

Materials and Methods

Figs. S1 to S10

Table S1

References (28-36)

Movies S1-S2

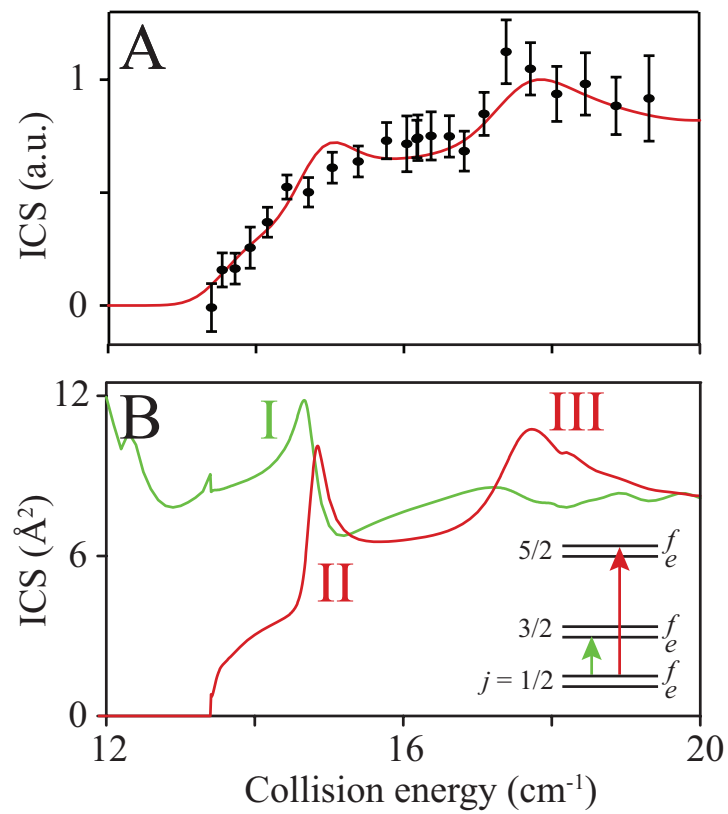


Figure 1:

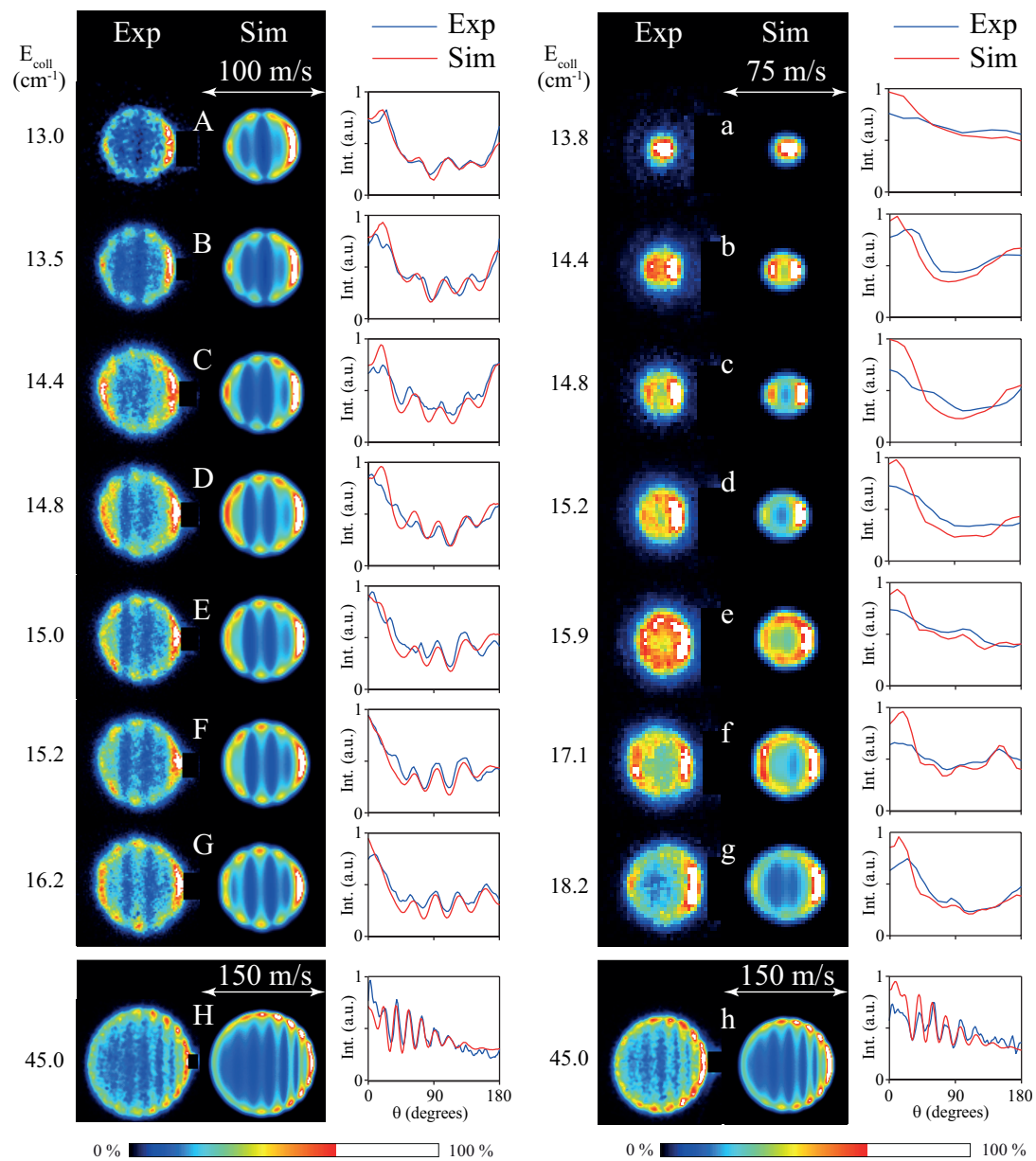
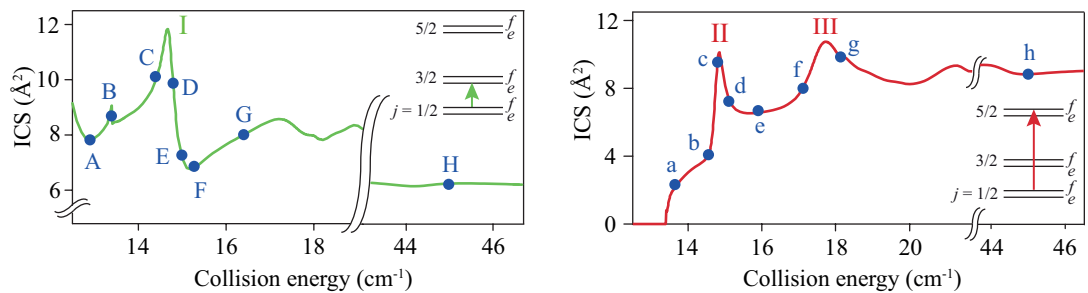


Figure 2:

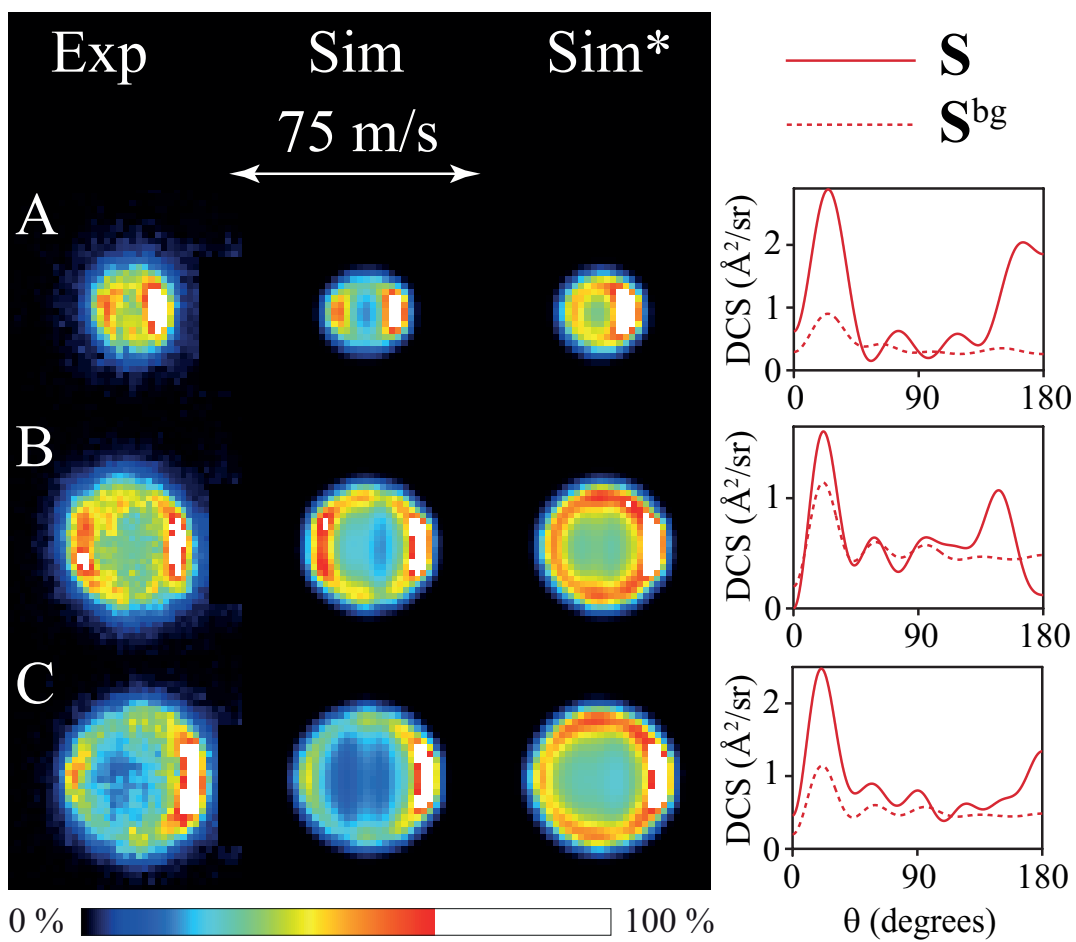
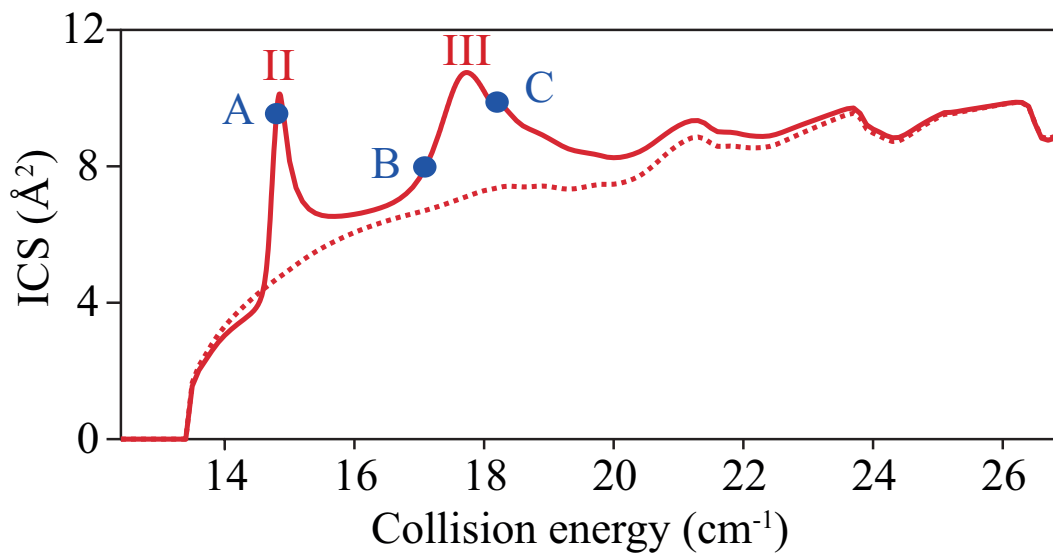


Figure 3:

Figure Captions:

Figure 1: Collision energy dependence of the integral cross section for rotational excitation of NO radicals by He atoms. (A) Comparison between measured (data points with error bars) and calculated (solid curve) state-to-state inelastic scattering cross sections for excitation into the $(5/2f)$ state. Experimental data in a.u., arbitrary units. Each data point is averaged over 1000 laser shots with the He and NO beams overlapping (collision signal), and 1000 laser shots with the NO beam only (reference signal). Vertical error bars represent statistical uncertainties at 95% of the confidence interval. The calculated cross section was convoluted with the experimental energy resolution of 0.3 cm^{-1} . (B) Calculated state-to-state integral cross sections for excitation into the $(3/2e)$ state (green curve) and $(5/2f)$ state (red curve). (Inset) Schematic energy level diagram and inelastic excitation scheme of NO.

Figure 2: Experimental (Exp) and simulated (Sim) ion images at selected collision energies as indicated in the top panels. Left panels: $(1/2f) \rightarrow (3/2e)$ inelastic collisions. Right panels: $(1/2f) \rightarrow (5/2f)$ inelastic collisions. The images are presented such that the relative velocity vector is oriented horizontally, with the forward direction on the right side of the image. Small segments of the images around forward scattering are masked due to imperfect state selection of the NO packet. The angular scattering distributions as derived from the experimental (blue curves) and simulated (red curves) images are shown for each channel and collision energy.

Figure 3: Effect of resonances II and III on the cross sections for inelastic $(1/2f) \rightarrow (5/2f)$ NO-He scattering. Integral cross sections are shown above, differential below. Solid lines represent the complete theoretical ICSs and DCSs, dashed lines the cross sections obtained

when only the scattering matrix \mathbf{S}^{bg} in Eq. (1) is included for resonances I, II, and III. The lower panels show the measured (Exp) and simulated images based on either the complete DCSs (Sim) or the DCSs computed with the scattering matrix \mathbf{S}^{bg} only (Sim*) for collision energies of (A) 14.8 cm^{-1} , (B) 17.1 cm^{-1} , and (C) 18.2 cm^{-1} . Fig. S10 shows resonance I in the $(1/2f) \rightarrow (3/2e)$ cross sections.